

ChemComm

Accepted Manuscript



This is an *Accepted Manuscript*, which has been through the Royal Society of Chemistry peer review process and has been accepted for publication.

Accepted Manuscripts are published online shortly after acceptance, before technical editing, formatting and proof reading. Using this free service, authors can make their results available to the community, in citable form, before we publish the edited article. We will replace this *Accepted Manuscript* with the edited and formatted *Advance Article* as soon as it is available.

You can find more information about *Accepted Manuscripts* in the [Information for Authors](#).

Please note that technical editing may introduce minor changes to the text and/or graphics, which may alter content. The journal's standard [Terms & Conditions](#) and the [Ethical guidelines](#) still apply. In no event shall the Royal Society of Chemistry be held responsible for any errors or omissions in this *Accepted Manuscript* or any consequences arising from the use of any information it contains.

Fluorescent vinblastine probes for live cell imaging.

Labros G. Meimetis,^{a**} Randy J. Giedt,^{a**} Hannes Mikula,^a Jonathan C. Carlson,^a Rainer H. Kohler,^a David B. Pirovich^a and Ralph Weissleder^{a,b}

Received 00th January 20xx,
Accepted 00th January 20xx

DOI: 10.1039/x0xx00000x

www.rsc.org/

Herein we describe the synthesis of several fluorescent analogues of the clinically approved microtubule destabilizing agent vinblastine. The evaluated probes are the most potent described and provides the first example of uptake, distribution and live cell imaging using this well known antimitotic agent.

Cytotoxic small molecule chemotherapeutics play an important role in cancer therapy. Microtubule targeting agents in particular, have been part of the medical armamentarium for many decades.¹ The vinca alkaloid class of natural products isolated from the Madagascar Periwinkle plant (*Catharanthus Roseus*) and their synthetic derivatives constitute the oldest and largest family of clinically approved anti-mitotic chemotherapeutic drugs.² They have found clinical application for lymphoma,³ non-small cell lung cancer,⁴ bladder cancer,⁵ breast cancer,⁶ myeloma,⁷ and melanoma.⁸ Despite their widespread clinical use, we still have an incomplete understanding of the pharmacokinetics and intracellular distribution of these compounds. We thus set out to develop cell permeable fluorescent versions of vinblastine to advance our understanding of this drug class in live cells.

Vinblastine binds at the tips of microtubules⁹ inhibiting polymerization and arresting cells in the G₂/M phase of mitosis. At higher concentrations vinblastine causes microtubule depolymerization and the formation of tubulin-vinblastine aggregates.¹⁰

More specifically, vinblastine binds at the interface between two α/β tubulin heterodimers with 80 % of its surface area buried in the complex (Figure 1).¹¹ A portion of the vindoline subgroup of vinblastine is solvent exposed and provides a suitable point for modification and fluorophore attachment.

Previously described fluorescent vinblastine conjugates employ derivatization at the C4 or C4' position.¹² Unfortunately, these first generation probes provided modest half maximal activity and failed to provide drug distribution in live cells. Based on structural analysis we reasoned that modification at the C3 position would be an alternative. We thus created a small library of compounds that differ in spacers and fluorochromes to identify the candidate with ideal imaging properties in live cells.

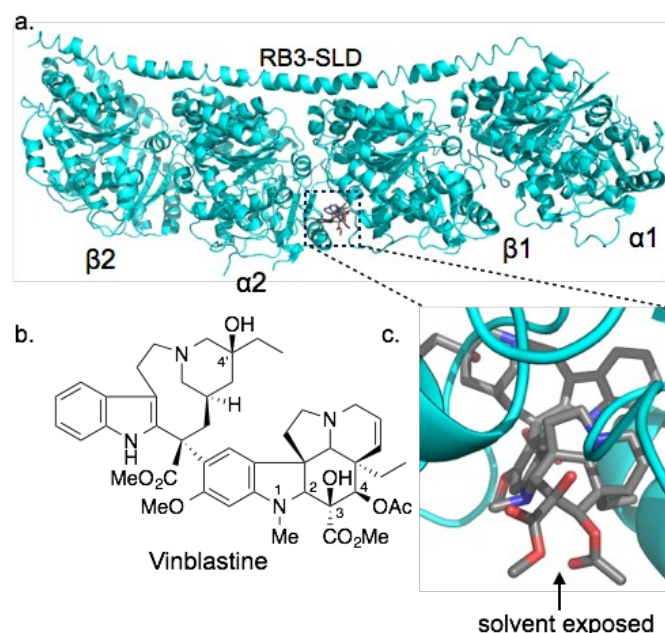


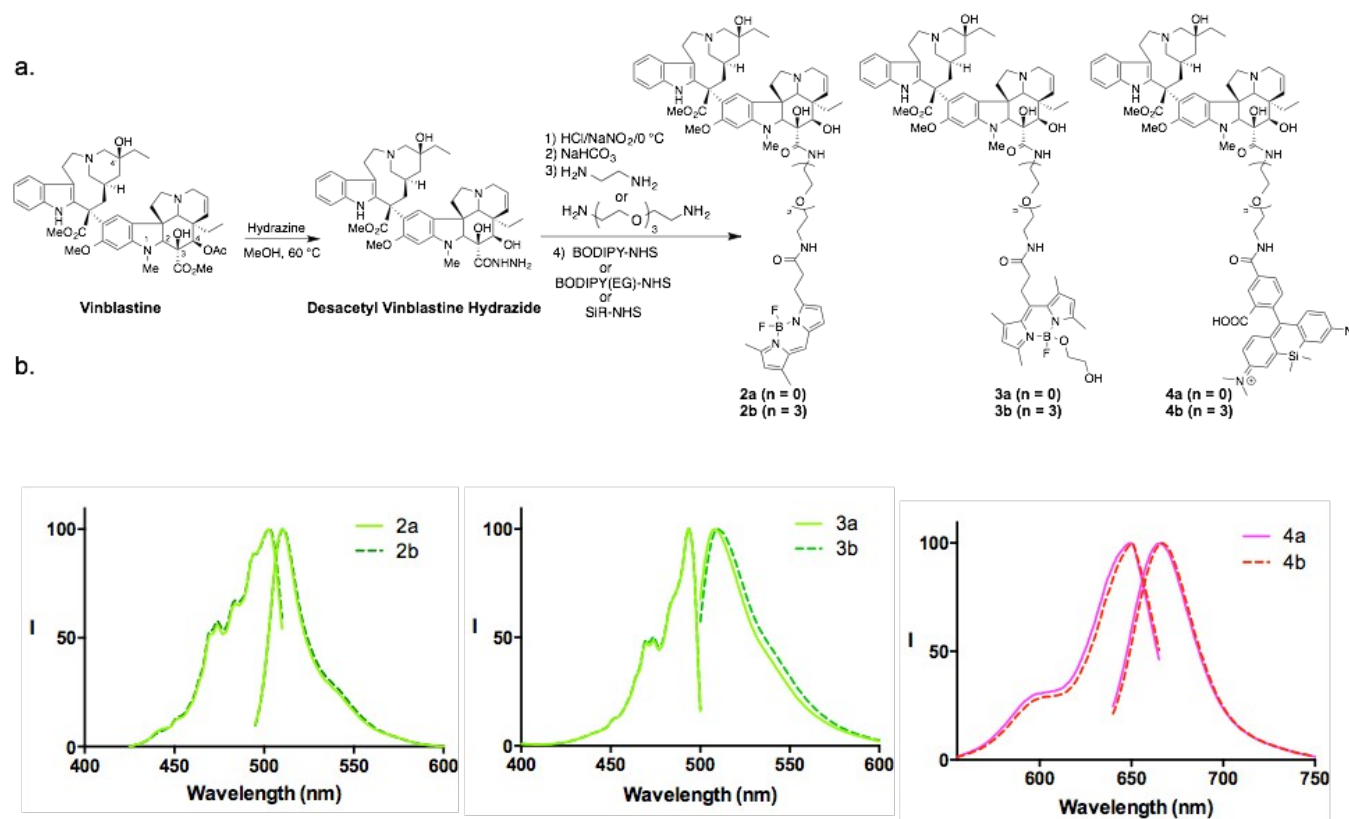
Figure 1 (a) Vinblastine bound between two α/β tubulin heterodimers (Protein Data Bank ID code 1Z2B). (b) Structure of vinblastine. (c) A portion of the vindoline subgroup is solvent exposed, providing a point for fluorophore attachment.

^a Center for Systems Biology, Massachusetts General Hospital, 185 Cambridge Street, CPZN 5206, Boston, Massachusetts 02114, United States.
E-mail: rweissleder@mgh.harvard.edu

^b Department of Systems Biology, Harvard Medical School, 200 Longwood Avenue, Boston, Massachusetts 02115, United States.

† These authors contributed equally to this body of work.

Electronic Supplementary Information (ESI) available: [details of any supplementary information available should be included here]. See DOI: 10.1039/x0xx00000x



Scheme 1 (a) Synthesis of vinblastine-fluorophore conjugates. (b) Excitation and emission spectra of vinblastine conjugates in phosphate buffered saline (PBS).

We began the synthesis by treating vinblastine with hydrazine in methanol at 60 °C to furnish desacetyl vinblastine hydrazide (Scheme 1).¹³ The hydrazide was then dissolved in 1 M HCl at 0 °C and stirred with sodium nitrite for 10 minutes, forming the corresponding acyl azide.¹⁴ This intermediate was immediately reacted with either ethylenediamine or 1,11,-diamino-3,6,9-trioxaundecane to give amines **1a** and **1b** respectively (see experimental). Varying the linker length between the drug and fluorophore has been shown to affect binding affinity and cellular distribution characteristics,¹⁵ therefore we selected a short (**1a**) and long (**1b**) linker to vary the SAR.

Appropriate fluorophores for live cell imaging must be bright, photostable and non-toxic. We selected the green emitting boron-dipyrrromethene based fluorophore (BODIPY) and the far-red emitting silicon-rhodamine (SiR) for conjugation. Both fluorophores have proven particularly successful for live cell imaging applications.¹⁶ Additionally, we incorporated the recently described boron-modified BODIPY variants (BODIPY-EG), which display enhanced water solubility, and a decreased propensity for getting trapped in lipophilic cellular compartments compared to its difluoro counterpart.¹⁷ To complete the syntheses, amines **1a** and **1b** were dissolved in a mixture of DMF and triethylamine to which was added the corresponding fluorophore-NHS. This yielded short and long linker vinblastine conjugates of BODIPY (**2a/2b**), BODIPY-EG

(**3a/3b**), and SiR (**4a/4b**). We evaluated the absorption and emission characteristics of the different probes at 1 μM in PBS (0.1 % DMSO). All three dyes display small Stokes shift and tight absorption and emission bands, characteristic of their respective fluorophore class (Scheme 1), which may be limiting in certain applications but have proven to be suitable for in vitro and in vivo imaging.¹⁶

Next, we measured the half maximal inhibitory concentration of the probes against the ovarian cancer cell line OVCA429 to determine the effect of linker length and dye selection (Figure 2). Live cells were incubated with the corresponding compound at different concentrations for 3 days followed by analysis using a PrestoBlue[®] cell viability assay (see experimental). Vinblastine (IC_{50} = 9.45 nM) proved to be the most potent followed by BODIPY conjugates **2a/2b** (IC_{50} = 30.2/43.0 nM). The SiR series **4a/4b** followed with IC_{50} = 140.7/180.7 nM. Interestingly, the BODIPY and SiR series display enhanced potency for the ethylenediamine derivatives over their PEG₃ spacer counterparts. Finally, conjugates **3a/3b** were the least effective (IC_{50} = 493.7/412.2 nM) and showed a reversal in inhibition with the long linker derivative **3b** being more potent than the short linker derivative **3a**. Commercially available C4 modified vinblastine-BODIPY (Figure S9, experimental section) had modest activity (IC_{50} = 247.5 nM).

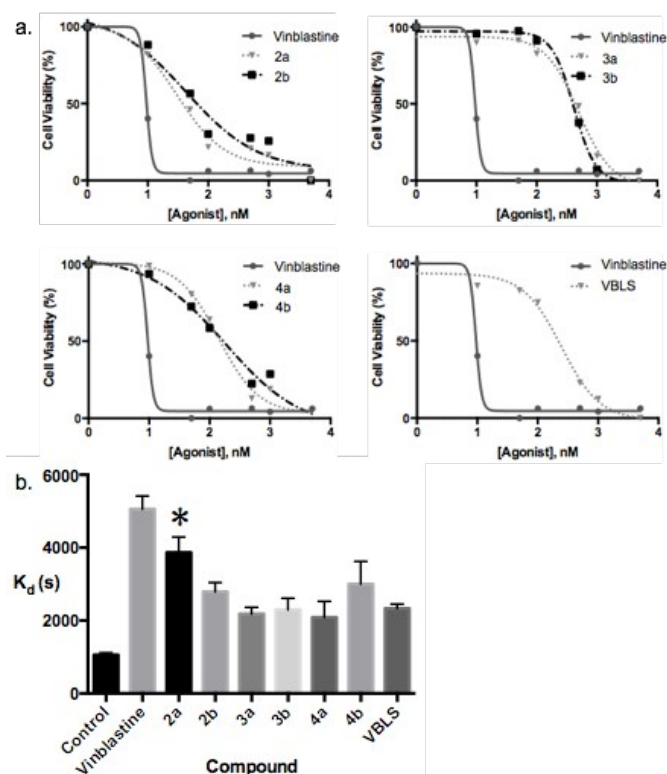


Figure 2 (a) IC₅₀ curves of vinblastine, vinblastine-fluorophores **2a/2b**, **3a/3b**, **4a/4b**, and commercially available vinblastine-BODIPY (VBLS) in OVCA429 cells using a fluorometric assay. (b) Plot of tubulin polymerization assay. K_d represents the time it takes to reach half maximal microtubule density with 2 μM of agonist (see experimental). * Non-significant compared to vinblastine.

Additionally, we evaluated the inhibitory effect the probes have on tubulin polymerization using a tubulin polymerization assay. It is based on the unique feature of DAPI (4',6-diamidino-2-phenylindole) fluorescence increasing upon binding to polymerized tubulin.¹⁸ We measured the time to achieve half maximal tubulin density at 2 μM of compound (K_d). Vinblastine was the most effective at inhibiting tubulin polymerization (K_d = 5056 s), followed by linker free BODIPY conjugate **2a** (K_d = 3869 s) and SiR-PEG₃ conjugate **4b** (K_d = 3001 s). Commercially available vinblastine-BODIPY had a modest effect with K_d = 2330 s, as did conjugates **3b**, **3a**, and **4a** with K_d = 2297, 2184 and 2089 s respectively.

Next, we acquired high-resolution images of the most potent conjugate **2a** at varying concentrations in the human fibrosarcoma cell line HT1080, transfected to express RFP tubulin (Figure 3).

At high probe concentration we observed the formation of microtubule paracrystals, a unique imaging phenotype specific to vinblastine.¹⁹ This occurs when microtubules depolymerize into vinca-bound α/β tubulin heterodimers followed by

reorganization to form birefringent uniaxial crystals.²⁰ At lower agonist concentrations of 10 μM and 1 μM probe **2a** causes microtubule depolymerisation into tubulin aggregates in addition to having cytoplasmic distribution. This confirms previous reports of vinblastines propensity to only bind microtubule tips, thus leading to the majority of intracellular drug being in an unbound state. Intrigued by the microtubule paracrystalline formation induced by probe **2a** we desired to observe the effects of the remaining probes on microtubule reorganization.

Probes **2b**, **3a/3b** and **4a/4b** were incubated in OVCA429 cells transfected with CellLight[®] tubulin-RFP, washed once with media then imaged (Figure 4). Average paracrystal length was determined using MATLAB software (see experimental). We observed the PEG₃ versions **2b**, **3b**, and **4b** provided a greater density and paracrystal length compared to their short linker counterpart's.

The PEG₃ analogue **2b** gave similar paracrystal size compared to native vinblastine (8.44 μm). The boron-modified BODIPY derivatives **3a** and **3b** also produced paracrystals. Unfortunately, both displayed an increased propensity for loss of signal (agonist) after washing when compared to their lipophilic counterparts **2a/2b**. This is most likely caused by the enhanced water solubility of the ethylene glycol modified BODIPY's and their decreased binding affinity. Interestingly, no paracrystal formation was observed in the silicon-rhodamine derivative **4a**. However, the cellular phenotype was observed in the PEG₃ analogue **4b** with dimensions comparable to the short linker counterpart's **2a/3a**. We hypothesize that the zwitterionic nature of the silicon rhodamine probe impedes paracrystal formation by providing non-favorable interactions between adjacent tubulin heterodimers.

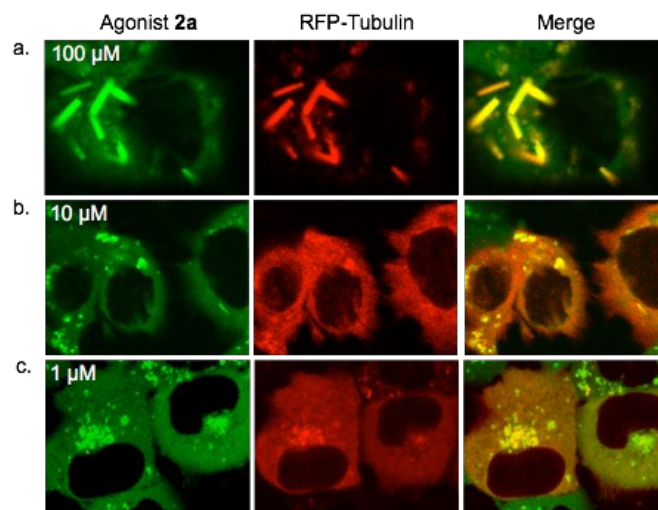


Figure 3 High-resolution live cell imaging of the most potent vinblastine conjugate **2a** in HT1080 cells expressing tubulin RFP. Cells were incubated for 3 h at (a) 100 μM (b) 10 μM, and (c) 1 h at 1 μM.

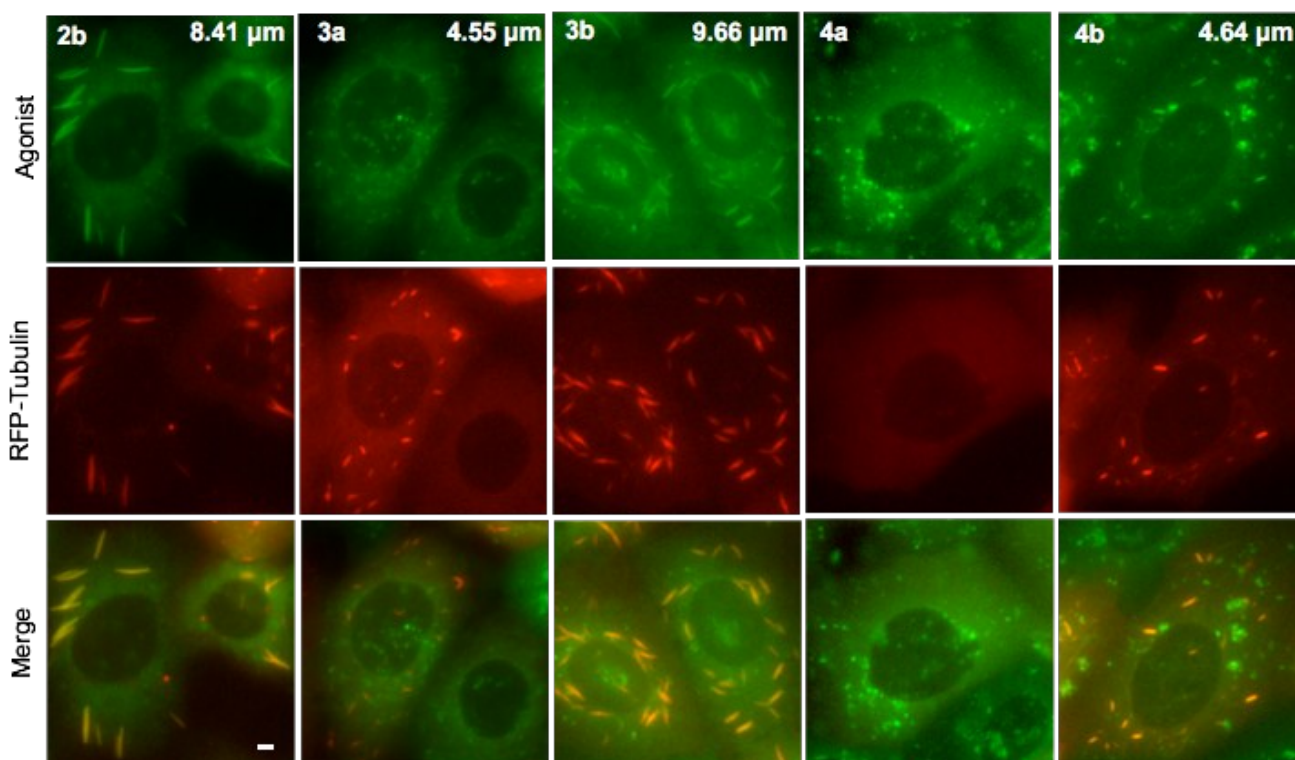


Figure 4 Live cell imaging of vinblastine-fluorophore conjugates in OVCA429 cells transfected with CellLight® RFP tubulin. The cells were incubated with 100 μM of probe for 3.5 h in media followed by a single wash and then imaged. Average paracrystal length is displayed at the top right. Bar = 10 μm .

In conclusion, we have designed and synthesized a small series of cell permeable vinblastine-fluorophore conjugates, several of which retain the potency of the therapeutic compound and provide the only live cell imaging and cellular distribution of this mitotic inhibitor. We envision these probes to find use in the study of single cell pharmacokinetics, pharmacodynamics and drug transport mechanisms. Finally, the vinblastine-SiR probe **4b** may find use in stimulated emission depletion (STED) microscopy to provide structural insight of microtubule reorganization by vinblastine.

This work was supported in part by the National Institutes of Health (NIH) grant 5R01EB010011-06 and the Department of Defense Breast Cancer Research Program BC134081.

Notes and references

- C. Dumontet and M. A. Jordan, *Nat. Rev. Drug. Discovery*, 2010, **9**, 790-803.
- R. L. Noble, C. T. Beer and J. H. Cutts, *Ann. NY. Acad. Sci.*, 1958, **76**, 882-894.
- D. M. Lucas, P. C. Still, L. B. Pérez, M. R. Grever and A. D. Kinghorn, *Curr. Drug. Targets*, 2010, **11**, 812-822.
- R. Ferrara, S. Pilotto, U. Peretti, M. Caccese, S. Kinspergher, L. Carbognin, N. Karachaliou, R. Rosell, G. Tortora and E. Bria, 2016. *Expert. Opin. Pharmacother*, 2016, 1-17.
- J. Bellmunt, C. Théodore, T. Demkov, B. Komyakov, L. Sengelov, G. Daugaard, A. Caty, J. Carles, A. Jagiello-Gruszfeld, O. Karyakin, F. M. Delgado, P. Hurteloup, E. Winqvist, N. Morsil, Y. Salhi, S. Culine and H. V. D. Maase, *J. Clin. Oncol*, 2009, **27**, 4454-4461.
- J. Bonnetterre and N. Penel, *Expert. Opin. Pharmacother*, 2008, **16**, 2901-2910.
- M. A. Hussein, *Oncologist*, 2003, **8**, 39-45.
- S. Bhatia, S. S. Tykodi and J. A. Thompson, *Oncology*, 2009, **23**, 488-496.
- L. Wilson, M. A. Jordan and A. Morse, *J. Mol. Biol.*, 1982, **159**, 125-149.
- J. A. Donoso, K. M. Haskins and R. H. Himes, *Cancer. Res*, 1979, **39**, 1604-1610.
- B. Gigant, C. Wang, R. B. G. Ravelli, F. Roussi, M. O. Steinmetz, P. A. Curmi, A. Sobel and M. Knossow, *Nature*, 2005, **435**, 519-522.
- S. K. Chatterjee, J. Laffray, P. Patel, R. Ravindra, Y. Qin, M. E. Kuehne and S. L. Bane, *Biochemistry*, 2002, **41**, 14010-14018; H. P. Eikesdal, W. Landuyt and O. Dahl, *Cancer. Lett.*, 2002, **178**, 209-217; S. S. Rai and J. Wolff, *FEBS. Lett.*, 1997, **416**, 251-253.
- C. J. Barnett, G. J. Cullinan, K. Gerzon, R. C. Hoying, W. E. Jones, W. M. Newlon, G. A. Poore, R. L. Robison, M. J. Sweeney and G. C. Todd, *J. Med. Chem.*, 1978, **21**, 88-96.
- R. A. Conrad, G. J. Cullinan, K. Gerzon, and G. A. Poore, *J. Med. Chem.*, 1979, **22**, 391-400.
- E. Kim, K. S. Yang, R. J. Giedt and R. Weissleder, *Chem. Comm*, 2014, **50**, 4504-4507.
- E. Kim, K. S. Yang, R. H. Kohler, J. M. Dubach, H. Mikula and R. Weissleder, *Bioconjug. Chem.*, 2015, **26**, 1513-1518; A. Turetsky, E. Kim, R. H. Kohler, M. A. Miller and R. Weissleder, *Sci. Rep.*, 2014, **4**, 1-7.
- A. M. Courtis, S. A. Santos, Y. Guan, A. J. Hendricks, B. Ghosh, M. D. Szantai-Kis, S. A. Reis, J. V. Shah and R. Mazitschek, *Bioconjug. Chem.*, 2014, **25**, 1043-1051.
- D. Bonne, C. Heusele, C. Simon and D. Pantaloni, *J. Biol. Chem.*, 1985, **260**, 2819-2825.
- Y. Nakamura and Y. Ishigaki, *Oncol. Lett.*, 2014, **8**, 2387-2392; N. Moiso, M. Erent, S. Whyte, S. Martin and P. M. Bayley, *J. Cell. Sci.*, 2002, **115**, 2367-2379; G. G. Gundersen, S. Khawaja, J. C. Bulinski, *J. Cell. Biol.*, 1987, **105**, 251-264.

Journal Name

COMMUNICATION

20 G. C. Na and S. N. Timasheff, *J. Biol. Chem.*, 1982, **257**, 10387-10391.

ChemComm Accepted Manuscript